A SPICE Model for Multiconductor Transmission Lines Excited by an Incident Electromagnetic Field

Clayton R. Paul, *Fellow, IEEE*

***Abstract*— This paper describes a SPICE model that may be used for predicting the time-domain or frequency-domain voltages and currents induced at the terminations of a multiconductor transmission line (MTL) by an incident electromagnetic field. Explicit results for the entries in the SPICE circuit model are obtained for an incident uniform plane wave that may represent sources such as radio and television transmitters, radars, lightning, etc. The result relies on the transformation of the MTL equations into uncoupled modal lines by similarity transformations. The entries in the similarity transformations are provided for lossless lines. The model is implemented using controlled sources to implement the modal transformations and delay lines to implement the modal lines. If the model is implemented as a SPICE subcircuit model, the time-domain form of the incident field can be implemented as a source external to that subcircuit model so that changes in the line responses due to changes in the incident field waveform can be simulated without changing the subcircuit model. In order to avoid negative line delays, the result is restricted to incident waves having components of the propagation vector in the positive direction along the line. This restriction can be removed by simply reversing the line. The paramount advantages of the model are that both time-domain and frequency-domain results can be easily obtained with the existing SPICE code, and nonlinear loads, such as transistors and digital devices, as well as dynamic loads, such as inductors and capacitors, may be easily incorporated using the existing elements in the SPICE code. Predicted results for MTL's using the method are compared to those of the time-domain to frequency-domain transformation and finite difference-time-domain (FDTD) methods.**

I. Introduction

ELECTROMAGNETIC fields from distant sources such as transmitters, lightning discharges, and an electromagnetic pulse (EMP), as well as nearby sources such as arcing at relay contacts can induce undesired signals at the endpoints of transmission lines which may cause detrimental effects in those termination networks. The traditional model of a transmission line is the distributed parameter, multiconductor transmission line (MTL) equations. These are a set of $(n+1)$ partial differential equations representing a line consisting of n conductors and a reference conductor for the line voltages. The line is considered to be a uniform line in that the $(n+1)$ conductors are parallel to each other and the z-axis of a rectangular coordinate system as shown in Fig. 1, and the cross-sectional dimensions and properties of the conductors and any inhomogeneous surrounding medium are constant along the line. The effects of the incident field are modeled as either distributed or lumped sources along the line in contrast to the usual crosstalk applications wherein the sources are lumped into the termination networks. These effects of the incident field appear as forcing functions on the right-hand side of the MTL equations. Incorporation of the effects of incident electromagnetic fields into the transmission line equations was considered for two-conductor lines in [1]–[6]. This was later extended to multiconductor lines in [7]–[14]. A digital computer program has been developed for the multiconductor case in the frequency domain [15]. The transmission-line formulation has been compared to the full-wave numerical solution in [16] and to experimental results in [17]. A literal solution for the two-wire case was obtained in [18]. The formulation has also been adapted to twisted pairs [19] and to shielded cables [20].

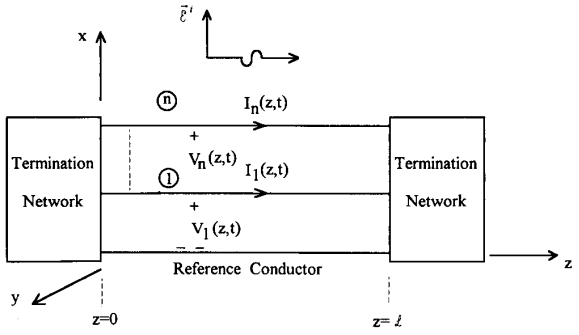

Fig. 1. The multiconductor transmission line (MTL) with incident field illumination.

The standard solution procedure is to obtain the general solution of the MTL equations and then incorporate the terminal network constraints into that general solution in order to determine the line voltages and currents at the ends of the line. The SPICE model presented in this paper essentially models the line as a $2n$-port independent of the terminations, and the terminal constraints (which may be nonlinear) are incorporated by connection at the $2n$ terminals of the SPICE overall model of the line. Thus nonlinear terminations can be incorporated in contrast to other methods which rely on superposition in computing the time-domain response. The currents that are modeled with these MTL equations are differential-mode or transmission-line currents, in that the sum of the currents directed in the $+z$ direction on all $(n+1)$ conductors is zero at every line cross section. In other words, the differential-mode currents of n of the conductors "return" on the reference conductor. In addition

Manuscript received September 9, 1993; revised May 13, 1994.

The author is with the Department of Electrical Engineering, University of Kentucky, Lexington, KY 40506 USA.

IEEE Log Number 9404490.

to these differential-mode currents, there can exist certain common-mode or antenna-mode currents that are not modeled by the MTL equations [3], [4], [21]–[23]. Hence, at points along the line there will be a combination of both currents only one component of which (the differential-mode) will be modeled by the MTL equations. If the MTL cross section is electrically small at the frequency of interest, the total current at the terminations is that predicted by the MTL equations. This is because for a line with electrically small cross-sectional dimensions, we can surround each termination with a closed surface (approximately a "node" in lumped-circuit analysis terminology), and Kirchhoff's current law shows that the total current entering this closed surface must be zero. Therefore, for a line having electrically small cross-sectional dimensions, the total current at the terminations must sum to zero (differential-mode or transmission-line current) so that the common-mode current not predicted by the MTL equations must go to zero at the terminations and is therefore of no importance in predicting the terminal responses of a MTL. This also applies to crosstalk on MTL's that have electrically small cross-sectional dimensions. Common-mode currents are important in modeling radiated emissions from the line or for MTL's where the terminations are not placed at the ends but at some intermediate point along the line such as a folded dipole antenna [6]. Therefore, the MTL equations we will solve provide the complete prediction of the terminal response of an MTL which satisfies the necessary requirement of electrically small cross-sectional dimensions.

The MTL equations were obtained in numerous references and are given by [1]–[13]

$$\frac{\partial}{\partial z}\boldsymbol{V}(z,t)+\boldsymbol{L}\frac{\partial}{\partial t}\boldsymbol{I}(z,t)+\boldsymbol{R}\boldsymbol{I}(z,t)=\boldsymbol{V}_F(z,t) \quad \text{(1a)}$$

$$\frac{\partial}{\partial z}\boldsymbol{I}(z,t)+\boldsymbol{C}\frac{\partial}{\partial t}\boldsymbol{V}(z,t)+\boldsymbol{G}V(z,t)=\boldsymbol{I}_F(z,t) \quad \text{(1b)}$$

where the $n \times n$ matrices $\boldsymbol{L},\boldsymbol{C},\boldsymbol{R},\boldsymbol{G}$ are the per-unit-length inductance, capacitance, resistance, and conductance matrices, respectively, that contain the cross-sectional dimensions and properties of the line, and t denotes the time variable. The line voltages (with respect to the reference conductor) and currents are contained in $V_i(z,t)=[\boldsymbol{V}(z,t)]_i$ and $I_i(z,t)=[\boldsymbol{I}(z,t)]_i$, respectively, for $i=1,\cdots,n$, where we denote the entry in the ith row of a vector $\boldsymbol{V}$ as $[\boldsymbol{V}]_i$. The $n \times 1$ vectors on the right-hand sides, $\boldsymbol{V}_F(z,t)$ and $\boldsymbol{I}_F(z,t)$, contain the effects of the incident fields and are determined by the components of the incident electric and magnetic fields that lie in the transverse plane (the x,y plane normal to the z-axis of the line). Denote a contour from the reference conductor to the ith conductor lying in the transverse (x,y) plane as c_i. The forcing functions $\boldsymbol{V}_F(z,t)$ and $\boldsymbol{I}_F(z,t)$, can be written as [1]–[13]

$$\boldsymbol{V}_F(z,t)=\frac{\partial}{\partial t}\boldsymbol{B}_N(z,t) \quad \text{(2a)}$$

$$\boldsymbol{I}_F(z,t)=-\boldsymbol{G}\boldsymbol{E}_T(z,t)-\boldsymbol{C}\frac{\partial}{\partial t}\boldsymbol{E}_T(z,t) \quad \text{(2b)}$$

where

$$[\boldsymbol{B}_N(z,t)]_i=\int_{c_i}\mathcal{B}^{\text{incident}}\cdot\vec{a}_n dl \quad (3)$$

and

$$[\boldsymbol{E}_T(z,t)]_i=\int_{c_i}\mathcal{E}^{\text{incident}}\cdot d\vec{l}. \quad (4)$$

The quantity $[\boldsymbol{B}_N(z,t)]_i$ is the integral of the component of the incident magnetic flux density vector that is in the transverse plane and normal to the contour c_i along that contour. The quantity $[\boldsymbol{E}_T(z,t)]_i$ is the integral of the component of the incident electric field intensity vector that is in the transverse plane and tangent to the contour c_i along that contour. Using Faraday's law [24], the forcing function $\boldsymbol{V}_F(z,t)$ can be equivalently expressed in terms of only the transverse and longitudinal electric fields as [1]–[13]

$$\boldsymbol{V}_F(z,t)=-\frac{\partial}{\partial z}\boldsymbol{E}_T(z,t)+\boldsymbol{E}_L(z,t) \quad \text{(2c)}$$

where

$$[\boldsymbol{E}_L(z,t)]_i=\mathcal{E}_z^{\text{incident}}(i\text{th conductor},z,t)-\mathcal{E}_z^{\text{incident}}(\text{reference conductor},z,t) \quad (5)$$

is the difference in the longitudinal (z-directed) components of the incident electric field intensity vector along the position of the ith conductor and along the position of the reference conductor (with those conductors absent).

For closely spaced conductors there is an additional term in (3) and (4) [10], [11]. These terms are produced by the induced quasi-static charge and current distributions on the line which have a net charge or current of zero on each conductor. For relatively widely spaced conductors, e.g., ratios of conductor separation to wire radius on the order of 5:1 and greater, these additional terms are apparently inconsequential so that a wide variety of practical line dimensions may be considered without the necessity for adding these terms. For simplicity, these additional terms necessary for closely spaced conductors will be omitted here. However, the formulation is sufficiently general that these source components may be added if desired.

The purpose of this paper is to provide a model for the general time-domain solution of these equations for incident uniform plane-wave illumination of the line that is implementable in standard circuit analysis codes such as SPICE. The model essentially represents the line, irrespective of the terminations, as a $2n$-port at its terminals. This form of representation has the important benefit that the terminations are incorporated in the overall SPICE model of the line external to the model of the conductors and so may be nonlinear. The utility of this result is that 1) the incorporation of the terminal constraints is obtained by the circuit analysis simulation code and one need not re-invent the numerical integration routines to solve the equations since these are built into those codes, and 2) models of a wide variety of linear and nonlinear circuit elements that can be used to model the termination networks are already available in those codes. In order to implement the model in a simple fashion, it is necessary to restrict the result to lossless lines, i.e., $\boldsymbol{R}=\boldsymbol{G}=\boldsymbol{0}$.

An additional contribution of this paper is to provide an explicit solution via the finite difference-time-domain (FDTD)

method. Although previous versions of this FDTD implementation have been presented in the literature by other researchers, the FDTD equations presented here represent a unique and stable implementation. We will compare the model predictions of the SPICE model presented here to those of the standard time-domain to frequency-domain transformation and the finite difference-time-domain (FDTD) solution in order to illustrate the limitations of these models.

II. Decoupling the MTL Equations

The MTL equations are *coupled* sets of partial differential equations. Perhaps the most common method for their solution is to *decouple* them with a similarity transformation. Consider the MTL equations for a lossless line

$$\frac{\partial}{\partial z}\boldsymbol{V}(z,t) = -\boldsymbol{L}\frac{\partial}{\partial t}\boldsymbol{I}(z,t) + \boldsymbol{V}_F(z,t) \tag{6a}$$

$$\frac{\partial}{\partial z}\boldsymbol{I}(z,t) = -\boldsymbol{C}\frac{\partial}{\partial t}\boldsymbol{V}(z,t) + \boldsymbol{I}_F(z,t). \tag{6b}$$

Define the transformation to *mode* quantities as

$$\boldsymbol{V}(z,t) = \boldsymbol{T}_V\boldsymbol{V}_m(z,t) \tag{7a}$$

$$\boldsymbol{I}(z,t) = \boldsymbol{T}_I\boldsymbol{I}_m(z,t). \tag{7b}$$

Substituting these into (6) gives

$$\frac{\partial}{\partial z}\boldsymbol{V}_m(z,t) = -\boldsymbol{L}_m\frac{\partial}{\partial t}\boldsymbol{I}_m(z,t) + \boldsymbol{V}_{Fm}(z,t) \tag{8a}$$

$$\frac{\partial}{\partial z}\boldsymbol{I}_m(z,t) = -\boldsymbol{C}_m\frac{\partial}{\partial t}\boldsymbol{V}_m(z,t) + \boldsymbol{I}_{Fm}(z,t) \tag{8b}$$

where $\boldsymbol{L}_m$ and $\boldsymbol{C}_m$ are the $n \times n$ matrices

$$\boldsymbol{L}_m = \boldsymbol{T}_V^{-1}\boldsymbol{L}\boldsymbol{T}_I \tag{9a}$$

$$\boldsymbol{C}_m = \boldsymbol{T}_I^{-1}\boldsymbol{C}\boldsymbol{T}_V \tag{9b}$$

and the incident field forcing functions for the *modes* become

$$\boldsymbol{V}_{Fm}(z,t) = \boldsymbol{T}_V^{-1}\boldsymbol{V}_F(z,t) \tag{10a}$$

$$\boldsymbol{I}_{Fm}(z,t) = \boldsymbol{T}_I^{-1}\boldsymbol{I}_F(z,t). \tag{10b}$$

If $\boldsymbol{T}_V$ and $\boldsymbol{T}_I$ can be chosen such that $\boldsymbol{L}_m$ and $\boldsymbol{C}_m$ are *diagonal* matrices, then the equations become uncoupled sets of two-conductor lines each with incident field excitation through elements of the vectors $\boldsymbol{V}_{Fm}(z,t)$ and $\boldsymbol{I}_{Fm}(z,t)$. This can always be done for lossless lines as was shown in [6]–[8]. So the basic solution technique utilizes the solution for a field-illuminated, lossless, two-conductor line.

This transformation is obtained by first determining an $n \times n$ real, orthogonal transformation $\boldsymbol{U}$ that diagonalizes $\boldsymbol{C}$ as

$$\boldsymbol{U}^t\boldsymbol{C}\boldsymbol{U} = \theta^2 \tag{11}$$

where θ^2 is a *diagonal matrix* and $\boldsymbol{U}^t$ denotes the *transpose* of $\boldsymbol{U}$. Since $\boldsymbol{C}$ is real and symmetric, this can always be done [6]–[8]. Furthermore, since $\boldsymbol{C}$ is positive definite, all elements of θ^2 are real and positive (and nonzero) so that we can form the square root of that matrix, θ, which will have real elements on its main diagonal and zeros elsewhere [6]–[8]. Next, find a real, orthogonal transformation $\boldsymbol{S}$ such that

$$\boldsymbol{S}^t\left(\theta\,\boldsymbol{U}^t\,\boldsymbol{L}\,\boldsymbol{U}\,\theta\right)\boldsymbol{S} = \Lambda^2 \tag{12}$$

where Λ^2 is again a *diagonal matrix* with real, positive elements on its diagonal. Define

$$\boldsymbol{T} = \boldsymbol{U}\,\theta\,\boldsymbol{S}. \tag{13}$$

Normalizing the columns of $\boldsymbol{T}$ to unity length gives

$$\boldsymbol{T}_{\text{norm}} = \boldsymbol{T}\,\alpha \tag{14}$$

where α is an $n \times n$ diagonal matrix. The above transformations can now be defined as

$$\boldsymbol{T}_I = \boldsymbol{U}\,\theta\,\boldsymbol{S}\,\alpha \tag{15}$$

$$\boldsymbol{T}_V = \boldsymbol{U}\,\theta^{-1}\,\boldsymbol{S}\,\alpha^{-1} \tag{16}$$

with the properties that

$$\begin{aligned}\boldsymbol{T}_V^{-1} &= \alpha^2\,\boldsymbol{T}_I^{-1}\,\boldsymbol{C}\\ &= \boldsymbol{T}_I^t.\end{aligned} \tag{17}$$

The modal per-unit-length parameter matrices given in (9) become

$$\begin{aligned}\boldsymbol{L}_m &= \boldsymbol{T}_V^{-1}\,\boldsymbol{L}\boldsymbol{T}_I\\ &= \boldsymbol{T}_I^t\,\boldsymbol{L}\boldsymbol{T}_I\\ &= \alpha^2\,\Lambda^2\end{aligned} \tag{18a}$$

$$\begin{aligned}\boldsymbol{C}_m &= \boldsymbol{T}_I^{-1}\,\boldsymbol{C}\boldsymbol{T}_V\\ &= \boldsymbol{T}_V^t\,\boldsymbol{C}\boldsymbol{T}_V\\ &= \alpha^{-2}.\end{aligned} \tag{18b}$$

Consequently, the mode characteristic impedances and velocities of propagation become

$$\begin{aligned}[\boldsymbol{Z}_{Cm}]_i &= Z_{Cmi}\\ &= \sqrt{\frac{l_{mi}}{c_{mi}}}\\ &= \alpha_i^2\Lambda_i\end{aligned} \tag{19a}$$

$$\begin{aligned}v_{mi} &= \frac{1}{\sqrt{l_{mi}c_{mi}}}\\ &= \frac{1}{\Lambda_i}.\end{aligned} \tag{19b}$$

III. The Frequency-Domain Solution

In order to obtain the time-domain solutions, we will transform the frequency-domain chain-parameter matrix to the time domain. The frequency-domain chain-parameter matrix relates the phasor voltages and currents at one end of the line to those at the other as [7]

$$\hat{\boldsymbol{V}}(\mathcal{L}) = \hat{\Phi}_{11}(\mathcal{L})\hat{\boldsymbol{V}}(0) + \hat{\Phi}_{12}(\mathcal{L})\hat{\boldsymbol{I}}(0) + \hat{\boldsymbol{V}}_{FT}(\mathcal{L}) \tag{20a}$$

$$\hat{\boldsymbol{I}}(\mathcal{L}) = \hat{\Phi}_{21}(\mathcal{L})\hat{\boldsymbol{V}}(0) + \hat{\Phi}_{22}(\mathcal{L})\hat{\boldsymbol{I}}(0) + \hat{\boldsymbol{I}_{FT}}(\mathcal{L}) \tag{20b}$$

where we denote the phasor quantities with a caret ($\hat{\boldsymbol{M}}$) and the total forcing functions are given by [7]

$$\hat{\boldsymbol{V}}_{FT}(\mathcal{L}) = \int_0^{\mathcal{L}}\left[\hat{\Phi}_{11}(\mathcal{L}-\tau)\hat{\boldsymbol{V}}_F(\tau) + \hat{\Phi}_{12}(\mathcal{L}-\tau)\hat{\boldsymbol{I}}_F(\tau)\right]d\tau \tag{21a}$$

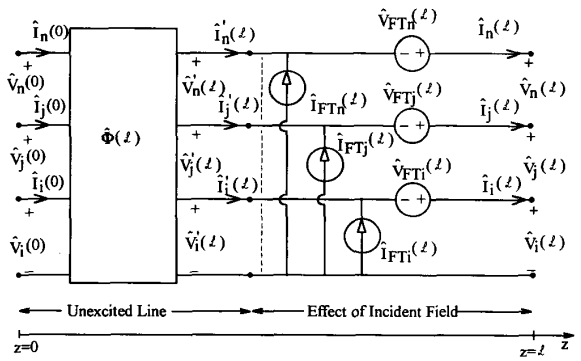

Fig. 2. Illustration of the interpretation of the model as the cascade of an unexcited line and sources representing the effects of the incident field.

$$\hat{I}_{FT}(\mathcal{L}) = \int_0^{\mathcal{L}} \left[\hat{\Phi}_{21}(\mathcal{L}-\tau)\hat{V}_F(\tau) + \hat{\Phi}_{22}(\mathcal{L}-\tau)\hat{I}_F(\tau)\right] d\tau. \tag{21b}$$

The chain-parameter submatrices are [7]

$$\hat{\Phi}_{11}(\mathcal{L}) = \frac{1}{2}\boldsymbol{C}^{-1}\boldsymbol{T}_I\left(e^{j\omega\Lambda\mathcal{L}} + e^{-j\omega\Lambda\mathcal{L}}\right)\boldsymbol{T}_I^{-1}\boldsymbol{C} \tag{22a}$$

$$\hat{\Phi}_{12}(\mathcal{L}) = -\frac{1}{2}\boldsymbol{C}^{-1}\boldsymbol{T}_I\Lambda\left(e^{j\omega\Lambda\mathcal{L}} - e^{-j\omega\Lambda\mathcal{L}}\right)\boldsymbol{T}_I^{-1} \tag{22b}$$

$$\hat{\Phi}_{21}(\mathcal{L}) = -\frac{1}{2}\boldsymbol{T}_I\left(e^{j\omega\Lambda\mathcal{L}} - e^{-j\omega\Lambda\mathcal{L}}\right)\Lambda^{-1}\boldsymbol{T}_I^{-1}\boldsymbol{C} \tag{22c}$$

$$\hat{\Phi}_{22}(\mathcal{L}) = \frac{1}{2}\boldsymbol{T}_I\left(e^{j\omega\Lambda\mathcal{L}} + e^{-j\omega\Lambda\mathcal{L}}\right)\boldsymbol{T}_I^{-1} \tag{22d}$$

where $e^{\pm j\omega\Lambda\mathcal{L}}$ are diagonal matrices with $e^{\pm j\omega\Lambda_i\mathcal{L}}$ on the main diagonals and $\boldsymbol{T}_I^{-1}\boldsymbol{C}\boldsymbol{L}\boldsymbol{T}_I = \Lambda^2$. The chain parameter matrix representation in (20) shows that we may view the problem as an unexcited line in series with sources representing the effects of the incident field as illustrated in Fig. 2.

Utilizing the forms of the chain parameter submatrices in (22) and the forms of the incident field forcing functions given in (2)–(5) one can show that (21) is equivalent to [7], [9]

$$\hat{V}_{FT}(\mathcal{L}) = \int_0^{\mathcal{L}} \hat{\Phi}_{11}(\mathcal{L}-z)\hat{E}_L(z)\,dz - \underbrace{\hat{\Phi}_{11}(0)}_{\mathbf{1}_n}\hat{E}_T(z=\mathcal{L}) + \hat{\Phi}_{11}(\mathcal{L})\hat{E}_T(z=0) \tag{23a}$$

where we have used the fact that $\hat{\Phi}_{11}(0) = \mathbf{1}_n$ where $\mathbf{1}_n$ is the $n \times n$ identity matrix. In a similar fashion one can show that

$$\hat{I}_{FT}(\mathcal{L}) = \int_0^{\mathcal{L}} \hat{\Phi}_{21}(\mathcal{L}-z)\hat{E}_L(z)\,dz - \underbrace{\hat{\Phi}_{21}(0)}_{\mathbf{0}}\hat{E}_T(z=\mathcal{L}) + \hat{\Phi}_{21}(\mathcal{L})\hat{E}_T(z=0) \tag{23b}$$

where we have used the property that $\hat{\Phi}_{21}(0) = \mathbf{0}$. The resulting forms for the total forcing functions given in the frequency domain in (23) show that they are a combination of the *convolution* of the longitudinal incident electric field terms plus the integral of the transverse incident electric fields at the ends of the line.

Transforming to mode quantities via (7) yields

$$\hat{V}_m(\mathcal{L}) = \hat{\Phi}_{m11}(\mathcal{L})\hat{V}_m(0) + \hat{\Phi}_{m12}(\mathcal{L})\hat{I}_m(0) + \hat{V}_{FTm}(\mathcal{L}) \tag{24a}$$

$$\hat{I}_m(\mathcal{L}) = \hat{\Phi}_{m21}(\mathcal{L})\hat{V}_m(0) + \hat{\Phi}_{m22}(\mathcal{L})\hat{I}_m(0) + \hat{I}_{FTm}(\mathcal{L}) \tag{24b}$$

where the modal chain-parameter submatrices become

$$\hat{\Phi}_{m11}(\mathcal{L}) = \boldsymbol{T}_V^{-1}\hat{\Phi}_{11}(\mathcal{L})\boldsymbol{T}_V = \frac{1}{2}\left(e^{j\omega\Lambda\mathcal{L}} + e^{-j\omega\Lambda\mathcal{L}}\right) \tag{25a}$$

$$\hat{\Phi}_{m12}(\mathcal{L}) = \boldsymbol{T}_V^{-1}\hat{\Phi}_{12}(\mathcal{L})\boldsymbol{T}_I = -\frac{1}{2}\underbrace{\alpha^2\Lambda}_{\boldsymbol{Z}_{Cm}}\left(e^{j\omega\Lambda\mathcal{L}} - e^{-j\omega\Lambda\mathcal{L}}\right) \tag{25b}$$

$$\hat{\Phi}_{m21}(\mathcal{L}) = \boldsymbol{T}_I^{-1}\hat{\Phi}_{21}(\mathcal{L})\boldsymbol{T}_V = -\frac{1}{2}\left(e^{j\omega\Lambda\mathcal{L}} - e^{-j\omega\Lambda\mathcal{L}}\right)\underbrace{\alpha^{-2}\Lambda^{-1}}_{\boldsymbol{Z}_{Cm}^{-1}} \tag{25c}$$

$$\hat{\Phi}_{m22}(\mathcal{L}) = \boldsymbol{T}_I^{-1}\hat{\Phi}_{22}(\mathcal{L})\boldsymbol{T}_I = \frac{1}{2}\left(e^{j\omega\Lambda\mathcal{L}} + e^{-j\omega\Lambda\mathcal{L}}\right) \tag{25d}$$

and the total modal forcing functions due to the incident field become

$$\hat{V}_{FTm}(\mathcal{L}) = \boldsymbol{T}_V^{-1}\hat{V}_{FT}(\mathcal{L}) = \int_0^{\mathcal{L}} \left[\frac{1}{2}\left(e^{j\omega\Lambda(\mathcal{L}-z)} + e^{-j\omega\Lambda(\mathcal{L}-z)}\right)\right] \times \boldsymbol{T}_I^t\hat{\boldsymbol{E}}_L(z)\,dz - \boldsymbol{T}_I^t\hat{\boldsymbol{E}}_T(\mathcal{L}) + \frac{1}{2}\left(e^{j\omega\Lambda(\mathcal{L})} + e^{-j\omega\Lambda(\mathcal{L})}\right) \times \boldsymbol{T}_I^t\hat{\boldsymbol{E}}_T(0) \tag{26a}$$

$$\hat{I}_{FTm}(\mathcal{L}) = \boldsymbol{T}_I^{-1}\hat{I}_{FT}(\mathcal{L}) = \int_0^{\mathcal{L}} \left[-\frac{1}{2}\left(e^{j\omega\Lambda(\mathcal{L}-z)} - e^{-j\omega\Lambda(\mathcal{L}-z)}\right) \times \boldsymbol{Z}_{Cm}^{-1}\boldsymbol{T}_I^t\hat{\boldsymbol{E}}_L(z)\right] dz - \frac{1}{2}\left(e^{j\omega\Lambda(\mathcal{L})} - e^{-j\omega\Lambda(\mathcal{L})}\right) \times \boldsymbol{Z}_{Cm}^{-1}\boldsymbol{T}_I^t\hat{\boldsymbol{E}}_T(0). \tag{26b}$$

IV. Uniform Plane-Wave Excitation of the Line

Although the above results are valid for any time form of the incident field excitation, a useful form is that of a uniform plane wave. Consider the line conductors located in the x, z plane and extending from $z = 0$ to $z = \mathcal{L}$ as shown in Fig. 3. The incident uniform plane wave is described by giving its direction of propagation in a spherical coordinate system via the angles θ_p and ϕ_p. The polarization of the electric field vector of the wave is specified by giving its angle, θ_E, relative to the unit vector in the ϕ direction, $\vec{a}_\phi$. The frequency-domain

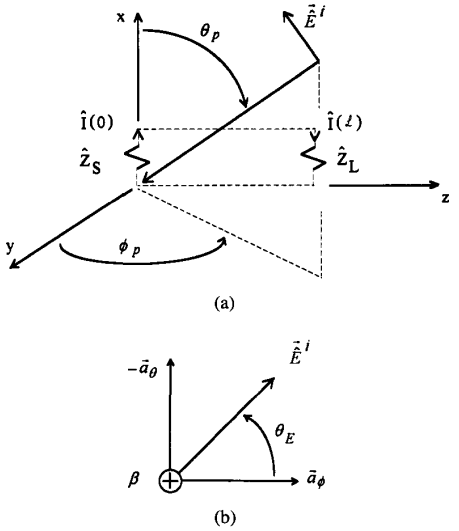

Fig. 3. Illustration of the definition of the incident field. (a) Propagation direction. (b) Electric-field polarization.

representation of the wave is [24]

$$\vec{\hat{E}}^{\,\text{incident}}(x,y,z,\omega) = \hat{E}_0(\omega)[e_x\vec{a}_x + e_y\vec{a}_y + e_z\vec{a}_z] \times e^{-j\beta_x x}e^{-j\beta_y y}e^{-j\beta_z z} \tag{27}$$

where the components of the incident electric field vector along the x, y, z axes of the rectangular coordinate system describing the line are

$$\begin{aligned} e_x &= \sin\theta_E \sin\theta_p \\ e_y &= -\sin\theta_E \cos\theta_p \cos\phi_p - \cos\theta_E \sin\phi_p \\ e_z &= -\sin\theta_E \cos\theta_p \sin\phi_p + \cos\theta_E \cos\phi_p. \end{aligned} \tag{28a}$$

The components of the phase constant along those coordinate axes are

$$\begin{aligned} \beta_x &= -\beta\cos\theta_p \\ \beta_y &= -\beta\sin\theta_p\cos\phi_p \\ \beta_z &= -\beta\sin\theta_p\sin\phi_p. \end{aligned} \tag{28b}$$

In the time domain, (27) translates to [24]

$$\vec{\mathcal{E}}^{\,\text{incident}}(x,y,z,t) = \mathcal{E}_0\left(t - \frac{x}{v_x} - \frac{y}{v_y} - \frac{z}{v_z}\right) \times [e_x\vec{a}_x + e_y\vec{a}_y + e_z\vec{a}_z]. \tag{29}$$

The time form of the electric field is denoted by $\mathcal{E}_0(t)$ which is the inverse Fourier transform of $\hat{E}_0(\omega)$, $\mathcal{E}_0(t) \Leftrightarrow \hat{E}_0(\omega)$, and the velocities of propagation along the axes are denoted by

$$\begin{aligned} v_x &= \frac{\omega}{\beta_x} = -\frac{v}{\cos\theta_p} \\ v_y &= \frac{\omega}{\beta_y} = -\frac{v}{\sin\theta_p\cos\phi_p} \\ v_z &= \frac{\omega}{\beta_z} = -\frac{v}{\sin\theta_p\sin\phi_p}. \end{aligned} \tag{30}$$

The frequency-domain contributions from the transverse and longitudinal components of this incident plane wave, $\hat{\boldsymbol{E}}_T(z)$ and $\hat{\boldsymbol{E}}_L(z)$, given in (4) and (5), can be evaluated in terms of the above results. If the reference conductor is placed at the origin of the coordinate system, $x = 0, y = 0$, as shown in Fig. 4(a), the transverse field contributions can be written in terms of the cross-sectional coordinates of the ith conductor (x_i, y_i) using the general form of the incident field in (27) as

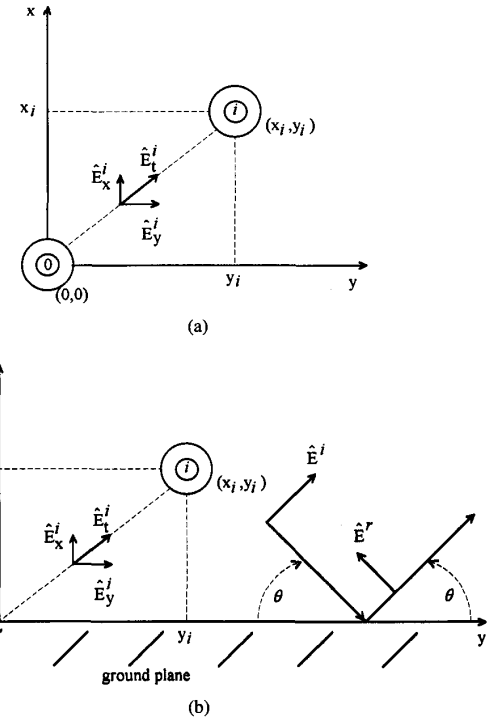

Fig. 4. Illustration of the computation of the induced sources for (a) $(n+1)$ conductors and (b) n conductors above an infinite, perfectly conducting ground plane.

$$\begin{aligned} \left[\hat{\boldsymbol{E}}_T(z)\right]_i &= \hat{E}_0(\omega)\int_0^{d_i}\left(e_x\frac{x_i}{d_i} + e_y\frac{y_i}{d_i}\right)e^{-j\beta_z z} \times e^{-j\left(\beta_x\frac{x_i}{d_i}+\beta_y\frac{y_i}{d_i}\right)\rho}d\rho \\ &= \hat{E}_0(\omega)[e_x x_i + e_y y_i]\frac{\sin(\psi_i)}{\psi_i} \times e^{-j\psi_i}e^{-j\beta_z z} \end{aligned} \tag{31a}$$

where $d_i = \sqrt{x_i^2 + y_i^2}$ is the straight-line distance between the reference conductor and the ith conductor in the transverse plane and

$$\psi_i = \frac{(\beta_x x_i + \beta_y y_i)}{2}. \tag{31b}$$

Similarly, the contributions due to the longitudinal field for the ith conductor are

$$\begin{aligned} \left[\hat{\boldsymbol{E}}_L(z)\right]_i &= \hat{E}_z^{\,\text{incident}}(x_i,y_i,z) - \hat{E}_z^{\,\text{incident}}(0,0,z) \\ &= -j(\beta_x x_i + \beta_x y_i)\hat{E}_0(\omega)e_z \times \frac{\sin(\psi_i)}{\psi_i}e^{-j\psi_i}e^{-j\beta_z z}. \end{aligned} \tag{32}$$

These results can be extended to the case where the reference conductor is an infinite, perfectly conducting ground plane located in the y, z plane at $x = 0$ as illustrated in Fig. 4(b). The total incident field is the sum of the incident field (with the ground plane and the other conductors removed) and the reflected field. Snell's law shows that the angles of incidence and reflection are the same [24]. Similarly, continuity of the tangential electric fields at the surface of the ground plane gives constraints on the y and z components of the electric field. Thus the incident and reflected (at the ground plane) fields are given by

$$\hat{\vec{E}}^{\text{incident}} = \hat{E}_0[e_x\vec{a}_x + e_y\vec{a}_y + e_z\vec{a}_z] \times e^{-j\beta_x x}e^{-j\beta_y y}e^{-j\beta_z z} \tag{33a}$$

$$\hat{\vec{E}}^{\text{reflected}} = \hat{E}_0[e_x\vec{a}_x - e_y\vec{a}_y - e_z\vec{a}_z] \times e^{j\beta_x x}e^{-j\beta_y y}e^{-j\beta_z z} \tag{33b}$$

and the total fields are

$$\hat{E}_x^{\text{Total}} = \hat{E}_x^{\text{ incident}} + \hat{E}_x^{\text{ reflected}} = 2\hat{E}_0 e_x \cos(\beta_x x)e^{-j\beta_y y}e^{-j\beta_z z} \tag{34a}$$

$$\hat{E}_y^{\text{Total}} = \hat{E}_y^{\text{ incident}} + \hat{E}_y^{\text{ reflected}} = -2j\hat{E}_0 e_y \sin(\beta_x x)e^{-j\beta_y y}e^{-j\beta_z z} \tag{34b}$$

$$\hat{E}_z^{\text{Total}} = \hat{E}_z^{\text{ incident}} + \hat{E}_z^{\text{ reflected}} = -2j\hat{E}_0 e_z \sin(\beta_x x)e^{-j\beta_y y}e^{-j\beta_z z}. \tag{34c}$$

The entries in the vectors in (4) and (5) become

$$\left[\hat{\boldsymbol{E}}_L(z)\right]_i = -2j\hat{E}_0(\omega)e_z\beta_x x_i\left[\frac{\sin(\beta_x x_i)}{\beta_x x_i}\right] \times e^{-j\beta_y y_i}e^{-j\beta_z z} \tag{35}$$

and

$$\left[\hat{\boldsymbol{E}}_T(z)\right]_i = \hat{E}_0(\omega)e^{-j\beta_z z}\left\{[e_x x_i + e_y y_i]\left[\frac{\sin(\psi_i^+)}{\psi_i^+}\right]e^{-j\psi_i^+} + [e_x x_i - e_y y_i]\left[\frac{\sin(\psi_i^-)}{\psi_i^-}\right]e^{-j\psi_i^-}\right\} \tag{36a}$$

where

$$\psi_i^{\pm} = \beta_x x_i \pm \beta_y y_i. \tag{36b}$$

V. The SPICE Equivalent Circuit

We now obtain the time-domain version of the chain-parameter representation. This will show how to construct a time-domain equivalent circuit that is implementable in the SPICE program. Substituting (25) into (24) yields

$$\hat{\boldsymbol{V}}_m(\mathcal{L}) = \frac{1}{2}\left(e^{j\omega\Lambda\mathcal{L}} + e^{-j\omega\Lambda\mathcal{L}}\right)\hat{\boldsymbol{V}}_m(0) - \frac{1}{2}\left(e^{j\omega\Lambda\mathcal{L}} - e^{-j\omega\Lambda\mathcal{L}}\right) \times \boldsymbol{Z}_{Cm}\hat{\boldsymbol{I}}_m(0) + \hat{\boldsymbol{V}}_{FTm}(\mathcal{L}) \tag{37a}$$

$$\boldsymbol{Z}_{Cm}\hat{\boldsymbol{I}}_m(\mathcal{L}) = -\frac{1}{2}\left(e^{j\omega\Lambda\mathcal{L}} - e^{-j\omega\Lambda\mathcal{L}}\right)\hat{\boldsymbol{V}}_m(0) + \frac{1}{2}\left(e^{j\omega\Lambda\mathcal{L}} + e^{-j\omega\Lambda\mathcal{L}}\right) \times \boldsymbol{Z}_{Cm}\hat{\boldsymbol{I}}_m(0) + \boldsymbol{Z}_{Cm}\hat{\boldsymbol{I}}_{FTm}(\mathcal{L}) \tag{37b}$$

and the mode characteristic impedance matrix (diagonal) is

$$\boldsymbol{Z}_{Cm} = \sqrt{\boldsymbol{L}_m\boldsymbol{C}_m^{-1}} = \alpha^2\Lambda.$$

Adding and subtracting these yields

$$\hat{\boldsymbol{V}}_m(0) - \boldsymbol{Z}_{Cm}\hat{\boldsymbol{I}}_m(0) = e^{-j\omega\Lambda\mathcal{L}}\left[\hat{\boldsymbol{V}}_m(\mathcal{L}) - \boldsymbol{Z}_{Cm}\hat{\boldsymbol{I}}_m(\mathcal{L})\right] + \hat{\boldsymbol{E}}_0(\mathcal{L}) \tag{38a}$$

$$\hat{\boldsymbol{V}}_m(\mathcal{L}) + \boldsymbol{Z}_{Cm}\hat{\boldsymbol{I}}_m(\mathcal{L}) = e^{-j\omega\Lambda\mathcal{L}}\left[\hat{\boldsymbol{V}}_m(0) + \boldsymbol{Z}_{Cm}\hat{\boldsymbol{I}}_m(0)\right] + \hat{\boldsymbol{E}}_{\mathcal{L}}(\mathcal{L}) \tag{38b}$$

where

$$\hat{\boldsymbol{E}}_0(\mathcal{L}) = -e^{-j\omega\Lambda\mathcal{L}}\left[\hat{\boldsymbol{V}}_{FTm}(\mathcal{L}) - \boldsymbol{Z}_{Cm}\hat{\boldsymbol{I}}_{FTm}(\mathcal{L})\right] \tag{39a}$$

$$\hat{\boldsymbol{E}}_{\mathcal{L}}(\mathcal{L}) = \left[\hat{\boldsymbol{V}}_{FTm}(\mathcal{L}) + \boldsymbol{Z}_{Cm}\hat{\boldsymbol{I}}_{FTm}(\mathcal{L})\right]. \tag{39b}$$

Recognizing the basic time-delay transformation

$$e^{\pm j\omega T}\hat{F}(\omega) \Leftrightarrow F(t \pm T) \tag{40}$$

these become, in the time domain,

$$\left[\boldsymbol{V}_m(0,t) - \boldsymbol{Z}_{Cm}\boldsymbol{I}_m(0,t)\right]_i = \left[\boldsymbol{V}_m(\mathcal{L}, t - T_i) - \boldsymbol{Z}_{Cm}\boldsymbol{I}_m(\mathcal{L}, t - T_i)\right]_i + \left[\boldsymbol{E}_0(\mathcal{L},t)\right]_i \tag{41a}$$

$$\left[\boldsymbol{V}_m(\mathcal{L},t) + \boldsymbol{Z}_{Cm}\boldsymbol{I}_m(\mathcal{L},t)\right]_i = \left[\boldsymbol{V}_m(0, t - T_i) + \boldsymbol{Z}_{Cm}\boldsymbol{I}_m(0, t - T_i)\right]_i + \left[\boldsymbol{E}_{\mathcal{L}}(\mathcal{L},t)\right]_i \tag{41b}$$

where the one-way time delay of the ith modal line is denoted by

$$T_i = \frac{\mathcal{L}}{v_{mi}} = \Lambda_i\mathcal{L}. \tag{42}$$

The additional sources are

$$[\boldsymbol{E}_0(\mathcal{L},t)]_i = -[\boldsymbol{V}_{FTm}(\mathcal{L}, t - T_i) - \boldsymbol{Z}_{Cm}\boldsymbol{I}_{FTm}(\mathcal{L}, t - T_i)]_i \tag{43a}$$

$$[\boldsymbol{E}_{\mathcal{L}}(\mathcal{L},t)]_i = [\boldsymbol{V}_{FTm}(\mathcal{L},t) + \boldsymbol{Z}_{Cm}\boldsymbol{I}_{FTm}(\mathcal{L},t)]_i. \tag{43b}$$

Equations (41) suggest the SPICE equivalent circuit for the modes that was developed for a line with no incident field illumination described in [6] but with the sources due to the incident field $[\boldsymbol{E}_0(\mathcal{L},t)]_i$ and $[\boldsymbol{E}_{\mathcal{L}}(\mathcal{L},t)]_i$ added to it. The transformation back to the actual line voltages and currents is accomplished with controlled sources that represent the mode transformations according to (7)

$$[\boldsymbol{V}(z,t)]_i = \sum_{k=1}^{n}\{[\boldsymbol{T}_V]_{ik}[\boldsymbol{V}_m(z,t)]_k\} \tag{44a}$$

$$[\boldsymbol{I}_m(z,t)]_i = \sum_{k=1}^{n}\left\{\left[\boldsymbol{T}_I^{-1}\right]_{ik}[\boldsymbol{I}(z,t)]_k\right\}. \tag{44b}$$

Thus the only difference between the SPICE model derived for the case of the excitation in the terminal networks and this case wherein the excitation is via an incident field is the

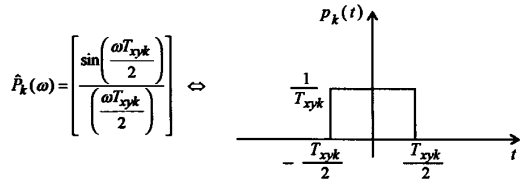

Fig. 5. Illustration of the pulse function that is involved in the time-domain convolution to determine the incident field sources.

implementation of the sources due to that field given in (41) and (43).

Substituting (26) into (39) the modal forcing functions become, in the frequency domain,

$$\begin{aligned}\hat{\boldsymbol{E}}_0(\mathcal{L}) &= -\boldsymbol{e}^{-j\omega\Lambda\mathcal{L}}\left[\hat{\boldsymbol{V}}_{FTm}(\mathcal{L}) - \boldsymbol{Z}_{Cm}\hat{\boldsymbol{I}}_{FTm}(\mathcal{L})\right] \\ &= -\int_0^{\mathcal{L}} \boldsymbol{e}^{-j\omega\Lambda\tau}\boldsymbol{T}_I^t\hat{\boldsymbol{E}}_L(\tau)d\tau \\ &\quad + \boldsymbol{e}^{-j\omega\Lambda\mathcal{L}}\boldsymbol{T}_I^t\hat{\boldsymbol{E}}_T(\mathcal{L}) - \boldsymbol{T}_I^t\hat{\boldsymbol{E}}_T(0) \qquad (45a)\\ \hat{\boldsymbol{E}}_{\mathcal{L}}(\mathcal{L}) &= \left[\hat{\boldsymbol{V}}_{FTm}(\mathcal{L}) + \boldsymbol{Z}_{Cm}\hat{\boldsymbol{I}}_{FTm}(\mathcal{L})\right] \\ &= \int_0^{\mathcal{L}} \boldsymbol{e}^{-j\omega\Lambda(\mathcal{L}-\tau)}\boldsymbol{T}_I^t\hat{\boldsymbol{E}}_L(\tau)d\tau \\ &\quad - \boldsymbol{T}_I^t\hat{\boldsymbol{E}}_T(\mathcal{L}) + \boldsymbol{e}^{-j\omega\Lambda\mathcal{L}}\boldsymbol{T}_I^t\hat{\boldsymbol{E}}_T(0). \qquad (45b)\end{aligned}$$

The time-domain equivalent of these modal forcing functions is obtained by transforming these frequency-domain forcing functions to the time domain by utilizing the basic time delay in (40) to yield

$$\begin{aligned}[\boldsymbol{E}_0(\mathcal{L},t)]_i &= \sum_{k=1}^{n}\left[\boldsymbol{T}_I^t\right]_{ik}\left\{-\int_0^{\mathcal{L}}\left[\boldsymbol{E}_L\left(z,t-\frac{z}{v_i}\right)\right]_k dz\right. \\ &\quad \left. + [\boldsymbol{E}_T(\mathcal{L},t-T_i)]_k - [\boldsymbol{E}_T(0,t)]_k\right\} \qquad (46a)\\ [\boldsymbol{E}_{\mathcal{L}}(\mathcal{L},t)]_i &= \sum_{k=1}^{n}\left[\boldsymbol{T}_I^t\right]_{ik}\left\{\int_0^{\mathcal{L}}\left[\boldsymbol{E}_L\left(z,t-T_i+\frac{z}{v_i}\right)\right]_k dz\right. \\ &\quad \left. - [\boldsymbol{E}_T(\mathcal{L},t)]_k - [\boldsymbol{E}_T(0,t-T_i)]_k\right\} \qquad (46b)\end{aligned}$$

where the mode velocities are $v_i = 1/\Lambda_i$ and the mode one-way delays are $T_i = \mathcal{L}/v_i = \Lambda_i\mathcal{L}$.

Although the above represents the most general form of the time variation of the incident field we will now specialize those results to the important case of an incident uniform plane wave whose characterization was determined in the preceeding section. First consider the case of no ground plane. Denote the cross-sectional time delay as

$$T_{xyk} = \frac{x_k}{v_x} + \frac{y_k}{v_y} \qquad (47)$$

and

$$T_z = \frac{\mathcal{L}}{v_z} \qquad (48)$$

along with the time delay of the modes, $T_i = \mathcal{L}/v_i = \Lambda_i\mathcal{L}$.

Substituting (31) and (32) into (45) yields

$$\begin{aligned}\left[\hat{\boldsymbol{E}}_0(\mathcal{L})\right]_i &= \hat{E}_0(\omega)\sum_{k=1}^{n}\left\{\left[\frac{\sin(\psi_k)}{\psi_k}\right]\left[\boldsymbol{T}_I^t\right]_{ik}\right. \\ &\quad \times \left[e_zT_{xyk}\mathcal{L} - (e_xx_k + e_yy_k)(T_i+T_z)\right] \\ &\quad \left.\times \frac{\left(e^{-j\omega\frac{T_{xyk}}{2}} - e^{-j\omega\left(T_i+T_z+\frac{T_{xyk}}{2}\right)}\right)}{(T_i+T_z)}\right\} \qquad (49a)\\ \left[\hat{\boldsymbol{E}}_{\mathcal{L}}(\mathcal{L})\right]_i &= \hat{E}_0(\omega)\sum_{k=1}^{n}\left\{\left[\frac{\sin(\psi_k)}{\psi_k}\right]\left[\boldsymbol{T}_I^t\right]_{ik}\right. \\ &\quad \times \left[e_zT_{xyk}\mathcal{L} + (e_xx_k + e_yy_k)(T_i-T_z)\right] \\ &\quad \left.\times \frac{\left(e^{-j\omega\left(T_i+\frac{T_{xyk}}{2}\right)} - e^{-j\omega\left(T_z+\frac{T_{xyk}}{2}\right)}\right)}{(T_i-T_z)}\right\}. \qquad (49b)\end{aligned}$$

Again, recognizing the basic time-delay transformation in (40), these sources transform to the time domain as

$$\begin{aligned}&[\boldsymbol{E}_0(\mathcal{L},t)]_i \\ &= \sum_{k=1}^{n}\left\{[e_zT_{xyk}\mathcal{L} - (e_xx_k + e_yy_k)(T_i+T_z)]\left[\boldsymbol{T}_I^t\right]_{ik}\right. \\ &\quad \left.\times p_k(t) * \frac{\mathcal{E}_0\left(t-\frac{T_{xyk}}{2}\right) - \mathcal{E}_0\left(t-T_i-T_z-\frac{T_{xyk}}{2}\right)}{(T_i+T_k)}\right\} \qquad (50a)\\ &[\boldsymbol{E}_{\mathcal{L}}(\mathcal{L},t)]_i \\ &= \sum_{k=1}^{n}\left\{[e_zT_{xyk}\mathcal{L} + (e_xx_k + e_yy_k)(T_i-T_z)]\left[\boldsymbol{T}_I^t\right]_{ik}\right. \\ &\quad \left.\times p_k(t) * \frac{\mathcal{E}_0\left(t-T_i-\frac{T_{xyk}}{2}\right) - \mathcal{E}_0\left(t-T_z-\frac{T_{xyk}}{2}\right)}{(T_i-T_k)}\right\} \qquad (50b)\end{aligned}$$

where $p_k(t)$ is the pulse function for the kth conductor given by

$$p_k(t) = \begin{cases} 0, & t < -\frac{T_{xyk}}{2} \\ \frac{1}{T_{xyk}}, & -\frac{T_{xyk}}{2} < t < \frac{T_{xyk}}{2} \\ 0, & t > -\frac{T_{xyk}}{2}\end{cases} \qquad (51)$$

as illustrated in Fig. 5 and $*$ denotes the *convolution* operation. Let us assume that the line cross-sectional dimensions are electrically small at the significant frequencies of the waveform $\mathcal{E}_0(t)$, so that $p_k(t)$ approximates an impulse

$$p_k(t) \cong \delta(t). \qquad (52)$$

Similarly, we will neglect the cross-sectional time delay in the $\mathcal{E}_0(t)$ expressions, $T_{xyk} \cong 0$ for all k, so that the forcing functions simplify to

$$\boldsymbol{E}_0(\mathcal{L},t) = \alpha_0\left[\frac{\mathcal{E}_0(t) - \mathcal{E}_0(t-T_i-T_z)}{(T_i+T_z)}\right] \qquad (53a)$$

$$\boldsymbol{E}_{\mathcal{L}}(\mathcal{L},t)=\alpha_{\mathcal{L}}\left[\frac{\mathcal{E}_0(t-T_i)-\mathcal{E}_0(t-T_z)}{(T_i-T_z)}\right] \tag{53b}$$

where the entries in the $n\times 1$ vectors α_0 and $\alpha_{\mathcal{L}}$ are given by

$$[\alpha_0]_i=\sum_{k=1}^{n}\left\{\left[e_zT_{xyk}\mathcal{L}-(e_xx_k+e_yy_k)(T_i+T_z)\right]\left[\boldsymbol{T}_I^t\right]_{ik}\right\} \tag{54a}$$

$$[\alpha_{\mathcal{L}}]_i=\sum_{k=1}^{n}\left\{\left[e_zT_{xyk}\mathcal{L}+(e_xx_k+e_yy_k)(T_i-T_z)\right]\left[\boldsymbol{T}_I^t\right]_{ik}\right\}. \tag{54b}$$

Therefore, the modal expressions in (41) simplify to

$$\begin{aligned}&[\boldsymbol{V}_m(0,t)-\boldsymbol{Z}_{Cm}\boldsymbol{I}_m(0,t)]_i\\&\quad=[\boldsymbol{V}_m(\mathcal{L},t-T_i)-\boldsymbol{Z}_{Cm}\boldsymbol{I}_m(\mathcal{L},t-T_i)]_i\\&\qquad+[\alpha_0]_i\left[\frac{\mathcal{E}_0(t)-\mathcal{E}_0(t-T_i-T_z)}{(T_i+T_z)}\right]\end{aligned} \tag{55a}$$

$$\begin{aligned}&[\boldsymbol{V}_m(\mathcal{L},t)+\boldsymbol{Z}_{Cm}\boldsymbol{I}_m(\mathcal{L},t)]_i\\&\quad=[\boldsymbol{V}_m(0,t-T_i)+\boldsymbol{Z}_{Cm}\boldsymbol{I}_m(0,t-T_i)]_i\\&\qquad+[\alpha_{\mathcal{L}}]_i\left[\frac{\mathcal{E}_0(t-T_i)-\mathcal{E}_0(t-T_z)}{(T_i-T_z)}\right]\end{aligned} \tag{55b}$$

Similar expressions for the case of a ground plane can be obtained by transforming (35) and (36). In fact, if we make the assumption that the line cross-sectional dimensions are electrically small at the significant frequencies of the waveform, then we may again use (53) and (54) but with modifications in α_0 and $\alpha_{\mathcal{L}}$: 1) they are multiplied by a factor of two and 2) we set $y_k=0$ for all k.

Equations (55) suggest the SPICE model shown in Fig. 6. The external nodes are denoted as $10i$ (at $z=0$) and $20i$ (at $z=\mathcal{L}$). Nodes $30i$, $40i$, $50i$, and $60i$ attach to controlled sources which implement the transformations between actual and mode quantities given in (44). The remainder of the network implements (55) for the ith mode. The controlled sources E_{0i} and $E_{\mathcal{L}i}$ implement (53) as

$$\begin{aligned}E_{0i}&=[\alpha_0]_i\left[\frac{\mathcal{E}_0(t)-\mathcal{E}_0(t-T_i-T_z)}{(T_i+T_z)}\right]\\&=\frac{[\alpha_0]_i}{(T_i+T_z)}[V(100)-V(96i)]\\E_{\mathcal{L}i}&=[\alpha_{\mathcal{L}}]_i\left[\frac{\mathcal{E}_0(t-T_i)-\mathcal{E}_0(t-T_z)}{(T_i-T_z)}\right]\\&=\frac{[\alpha_{\mathcal{L}}]_i}{(T_i-T_z)}[V(95i)-V(97i)].\end{aligned}$$

The five delay lines simulating (55) for each mode need not be terminated in the mode characteristic impedances but can be terminated in any characteristic impedance in order to remove reflections and give the desired ideal delay of $\mathcal{E}_0(t)$. If the wave has no propagation component in the z direction, $T_z=0$, then the last two lines are removed from the model. If the wave has a component in the $+z$ direction, it may happen that $T_i=T_z$ in which case (55b) appears to be undefined. However, this term becomes

$$\left[\frac{\mathcal{E}_0(t-T_i)-\mathcal{E}_0(t-T_z)}{(T_i-T_z)}\right]_{T_z\to T_i}=-\frac{d}{dt}\mathcal{E}_0(t-T_i) \tag{56}$$

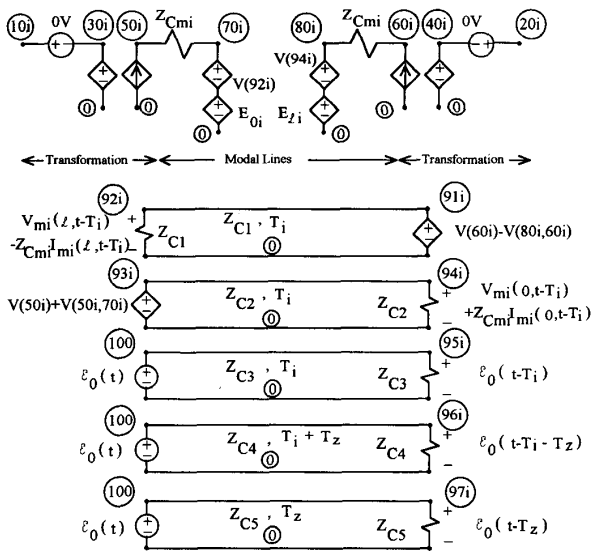

Fig. 6. Illustration of the SPICE model for the ith modal line.

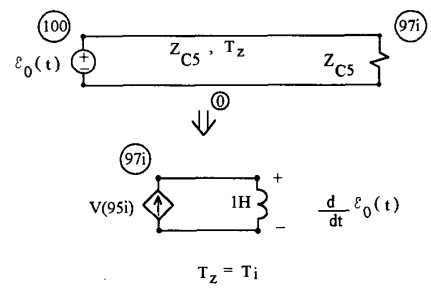

Fig. 7. Replacement of the delay line in the special case where the incident-field is propagating along the line axis.

so that the last delay line is replaced as shown in Fig. 7 and $E_{\mathcal{L}i}$ becomes

$$\begin{aligned}E_{\mathcal{L}i}&=[\alpha_{\mathcal{L}}]_i\left[\frac{\mathcal{E}_0(t-T_i)-\mathcal{E}_0(t-T_z)}{(T_i-T_z)}\right]\\&=-[\alpha_{\mathcal{L}}]_i[V(97i)].\end{aligned}$$

Waves having a component in the $-z$ direction, may result in the last two delay lines having negative delays which SPICE does not allow. Thus we must restrict this model to positive T_z. For negative T_z simply reverse the ends of the model.

The SPICE model shown in Fig. 6 requires five delay lines in order to implement (55) for each mode. The original SPICE model for a two-conductor line implements the required delays of the first two delay lines in the internal coding for the line. If one has access to the SPICE source code, the five delay lines in Fig. 6 can be implemented simply in the software by using two controlled sources having the dependences in (55) and the code then recompiled. Ordinarily, users do not have such access so in order to accommodate a wide class of users, the model of Fig. 6, while lengthy, can be implemented using the available SPICE element models without resorting to rewriting the SPICE source code.

VI. Time-Domain to Frequency-Domain Transformations

Perhaps the most straightforward method of obtaining the time-domain response is to view the problem as a 2-port with $\mathcal{E}_0(t)$ as the input and the desired terminal response voltage (or current) as the output. The magnitude and phase of $\mathcal{E}_0(t)$ can be obtained with the Fourier transform or can be approximated as a periodic waveform with a sufficiently long period [25]. The frequency-domain transfer function can be obtained by incorporating the terminal constraints into the chain parameter representation [6], [7]. The magnitudes of the spectral components of $\hat{E}_0(\omega)$ are multiplied with the magnitude of the transfer function, and the phase angles of $\hat{E}_0(\omega)$ are added to the phase angles of the transfer function to produce the magnitude and phase of the response. Then the inverse Fourier transform can be used to convert this back to the time domain [25].

The method is straightforward and can handle $\sqrt{f}$ skin-effect losses. However, it relies on superposition so that the 2-port must be linear. This means that the line terminations as well as the surrounding medium must be *linear*. Therefore, nonlinear loads as well as corona breakdown in lightning studies cannot be handled with this method.

VII. Finite-Difference Time-Domain Methods

Another straightforward way of (approximately) solving the MTL equations is with the finite-difference time-domain (FDTD) method. The FDTD discretization of the transmission-line equations for crosstalk predictions (no incident field illumination) was obtained in [26]. FDTD derivations and discretizations for incident field illumination are given in [13] and [27]–[29]. The space and time dimensions are discretized as Δz and Δt, respectively, giving a recursion relation in the form of a set of difference equations. The transmission-line equations in (1) become

$$\frac{\partial}{\partial z}\boldsymbol{V}(z,t)+\boldsymbol{R}\boldsymbol{I}(z,t)+\boldsymbol{L}\frac{\partial}{\partial t}\boldsymbol{I}(z,t) = -\frac{\partial}{\partial z}\boldsymbol{E}_T(z,t)+\boldsymbol{E}_L(z,t)+\boldsymbol{V}'_F(z,t) \quad (57a)$$

$$\frac{\partial}{\partial z}\boldsymbol{I}(z,t)+\boldsymbol{G}\boldsymbol{V}(z,t)+\boldsymbol{C}\frac{\partial}{\partial t}\boldsymbol{V}(z,t) = -\frac{\partial}{\partial t}\boldsymbol{C}E_T(z,t)+\boldsymbol{I}'_F(z,t) \quad (57b)$$

where the $n\times 1$ vectors $\boldsymbol{E}_T$ and $\boldsymbol{E}_L$ are due to the transverse and longitudinal components of the incident electric field. The vectors $\boldsymbol{V}'_F(z,t)$ and $\boldsymbol{I}'_F(z,t)$ are used to model lumped sources along the line such as at the terminations as described in [26]. The vectors $\boldsymbol{E}_T$ and $\boldsymbol{E}_L$ were given, in the frequency domain, in (31) and (32) for the case of no ground plane. Assuming the line cross-sectional dimensions are electrically small at the significant frequencies of $\mathcal{E}_0(t)$, we obtain

$$\left[-\frac{\partial}{\partial z}\hat{\boldsymbol{E}}_T(z)+\hat{\boldsymbol{E}}_L(z)\right]_i = j\omega\left[\frac{1}{v_z}(e_x x_i+e_y y_i)-\left(\frac{x_i}{v_x}+\frac{y_i}{v_y}\right)e_z\right]\hat{E}_0(\omega)e^{-j\beta_z z}. \quad (58)$$

This translates in the time domain to

$$-\frac{\partial}{\partial z}\boldsymbol{E}_T(z,t)+\boldsymbol{E}_L(z,t)=\left[\frac{1}{v_z}\boldsymbol{A}_T-\boldsymbol{A}_L\right]\frac{\partial}{\partial z}\mathcal{E}_0\left(t-\frac{z}{v_z}\right) \quad (59)$$

where

$$\left[\boldsymbol{A}_T\right]_i=(e_x x_i+e_y y_i) \quad (60a)$$

$$\left[\boldsymbol{A}_L\right]_i=\left(\frac{x_i}{v_x}+\frac{y_i}{v_y}\right)e_z. \quad (60b)$$

Similarly

$$-\frac{\partial}{\partial t}\boldsymbol{C}E_T(z,t)=-\boldsymbol{C}\boldsymbol{A}_T\frac{\partial}{\partial t}\mathcal{E}_0\left(t-\frac{z}{v_z}\right). \quad (61)$$

The line is discretized into NDZ $=\mathcal{L}/\Delta z$ sections of length Δz. The voltage and current solution points are interlaced one-half cell apart as described in [26] for stability purposes. Similarly, the voltage and current solution times are also interlaced one-half time step apart as as described in [26]. Thus the voltages and currents are denoted as $V_k^n\equiv V((k-1)\Delta z,n\Delta t)$ and $I_k^{n+1/2}\equiv I((k-1/2)\Delta z,(n+1/2)\Delta t)$ where k and n are integers. In other words, the voltage locations are at $0,\Delta z,2\Delta z,\cdots$ and the current locations are at $\Delta z/2,3\Delta z/2,5\Delta z/2,\cdots$. Similarly, the time points for the voltages are at $0,\Delta t,2\Delta t,\cdots$, and the time points for the currents are at $\Delta t/2,3\Delta t/2,5\Delta t/2,\cdots$. Using this scheme, the difference equations become

$$\begin{aligned}&\frac{1}{\Delta z}\left[\boldsymbol{V}_{k+1}^{n+1}-\boldsymbol{V}_k^{n+1}\right]+\frac{1}{\Delta t}\boldsymbol{L}\left[\boldsymbol{I}_k^{n+3/2}-\boldsymbol{I}_k^{n+1/2}\right]\\&\quad+\frac{1}{2}\boldsymbol{R}\left[\boldsymbol{I}_k^{n+3/2}+\boldsymbol{I}_k^{n+1/2}\right]\\&\quad=\left[\frac{1}{v_z}\boldsymbol{A}_T-\boldsymbol{A}_L\right]\frac{1}{\Delta t}\left[\mathcal{E}_0\left(t^{n+3/2}-\frac{(k-1/2)\Delta z}{v_z}\right)\right.\\&\quad\quad\left.-\mathcal{E}_0\left(t^{n+1/2}-\frac{(k-1/2)\Delta z}{v_z}\right)\right]\\&\quad\quad+\frac{1}{2}\left[\boldsymbol{V}'^{n+3/2}_{Fk}+\boldsymbol{V}'^{n+1/2}_{Fk}\right]\end{aligned} \quad (62a)$$

$$\begin{aligned}&\frac{1}{\Delta z}\left[\boldsymbol{I}_k^{n+1/2}-\boldsymbol{I}_{k-1}^{n+1/2}\right]+\frac{1}{\Delta t}\boldsymbol{C}\left[\boldsymbol{V}_k^{n+1}-\boldsymbol{V}_k^{n}\right]\\&\quad+\frac{1}{2}\boldsymbol{G}\left[\boldsymbol{V}_k^{n+1}+\boldsymbol{V}_k^{n}\right]\\&\quad=-\boldsymbol{C}\boldsymbol{A}_T\frac{1}{\Delta t}\left[\mathcal{E}_0\left(t^{n+1}-\frac{(k-1)\Delta z}{v_z}\right)\right.\\&\quad\quad\left.-\mathcal{E}_0\left(t^{n}-\frac{(k-1)\Delta z}{v_z}\right)\right]\\&\quad\quad+\frac{1}{2}\left[\boldsymbol{I}'^{n+1}_{Fk}+\boldsymbol{I}'^{n}_{Fk}\right].\end{aligned} \quad (62b)$$

Rearranging these gives

$$\begin{aligned}&\left[\frac{1}{\Delta t}\boldsymbol{C}+\frac{1}{2}\boldsymbol{G}\right]\boldsymbol{V}_k^{n+1}\\&\quad=\left[\frac{1}{\Delta t}\boldsymbol{C}-\frac{1}{2}\boldsymbol{G}\right]\boldsymbol{V}_k^{n}-\frac{1}{\Delta z}\left[\boldsymbol{I}_k^{n+1/2}-\boldsymbol{I}_{k-1}^{n+1/2}\right]\\&\quad\quad-\boldsymbol{C}\boldsymbol{A}_T\frac{1}{\Delta t}\left[\mathcal{E}_0\left(t^{n+1}-\frac{(k-1)\Delta z}{v_z}\right)\right.\\&\quad\quad\left.-\mathcal{E}_0\left(t^{n}-\frac{(k-1)\Delta z}{v_z}\right)\right]+\frac{1}{2}\left[\boldsymbol{I}'^{n+1}_{Fk}+\boldsymbol{I}'^{n}_{Fk}\right]\end{aligned} \quad (63a)$$

$$\left[\frac{1}{\Delta t}\boldsymbol{L}+\frac{1}{2}\boldsymbol{R}\right]\boldsymbol{I}_k^{n+3/2} = \left[\frac{1}{\Delta t}\boldsymbol{L}-\frac{1}{2}\boldsymbol{R}\right]\boldsymbol{I}_k^{n+1/2}-\frac{1}{\Delta z}\left[\boldsymbol{V}_{k+1}^{n+1}-\boldsymbol{V}_k^{n+1}\right] + \left[\frac{1}{v_z}\boldsymbol{A}_T-\boldsymbol{A}_L\right]\frac{1}{\Delta t}\left[\mathcal{E}_0\left(t^{n+3/2}-\frac{(k-1/2)\Delta z}{v_z}\right)-\mathcal{E}_0\left(t^{n+1/2}-\frac{(k-1/2)\Delta z}{v_z}\right)\right] + \frac{1}{2}\left[\boldsymbol{V}_{Fk}'^{n+3/2}+\boldsymbol{V}_{Fk}'^{n+1/2}\right]. \quad (63b)$$

The terminal conditions are characterized as resistive in the form of Generalized Thevenin Equivalents as

$$\boldsymbol{V}(0,t)=\boldsymbol{V}_S-\boldsymbol{R}_S\boldsymbol{I}(0,t) \quad (64a)$$
$$\boldsymbol{V}(\mathcal{L},t)=\boldsymbol{V}_L+\boldsymbol{R}_L\boldsymbol{I}(\mathcal{L},t). \quad (64b)$$

First the line voltages are solved for from (63a). As described in [26], we let $\boldsymbol{I}_0=\boldsymbol{0}, \boldsymbol{G}=(1/\Delta z)\boldsymbol{R}_S^{-1}, \boldsymbol{I}_F'=(1/\Delta z)\boldsymbol{R}_S^{-1}\boldsymbol{V}_S$ along with replacing $\boldsymbol{C}$ with $(1/2)\boldsymbol{C}$ for $k=1$ to yield

$$\boldsymbol{V}_1^{n+1}=\left[\frac{\Delta z}{\Delta t}\boldsymbol{R}_S\boldsymbol{C}+\boldsymbol{1}\right]^{-1}\left\{\left[\frac{\boldsymbol{\Delta z}}{\boldsymbol{\Delta t}}\boldsymbol{R}_S\boldsymbol{C}-\boldsymbol{1}\right]\boldsymbol{V}_1^{n}-2\boldsymbol{R}_S \times\left[\boldsymbol{I}_1^{n+1/2}-\underbrace{\boldsymbol{I}_o^{n+1/2}}_{0}\right] -\frac{\Delta z}{\Delta t}\boldsymbol{R}_S\boldsymbol{C}\boldsymbol{A}_T\left[\mathcal{E}_0\left(t^{n+1}\right)-\mathcal{E}_0(t^n)\right] +\left[\boldsymbol{V}_S^{n+1}+\boldsymbol{V}_S^{n}\right]\right\}. \quad (65a)$$

For $k=2,\cdots,$ NDZ we obtain

$$\boldsymbol{V}_k^{n+1}=\boldsymbol{V}_k^{n}-\frac{\Delta t}{\Delta z}\boldsymbol{C}^{-1}\left[\boldsymbol{I}_k^{n+1/2}-\boldsymbol{I}_{k-1}^{n+1/2}\right] -\boldsymbol{A}_T\left[\mathcal{E}_0\left(t^{n+1}-\frac{(k-1)\Delta z}{v_z}\right)-\mathcal{E}_0\left(t^{n}-\frac{(k-1)\Delta z}{v_z}\right)\right]. \quad (65b)$$

Similarly, we let $\boldsymbol{I}_{\mathrm{NDZ}+1}=\boldsymbol{0}, \boldsymbol{G}=(1/\Delta z)\boldsymbol{R}_L^{-1}, \boldsymbol{I}_F'=(1/\Delta z)\boldsymbol{R}_L^{-1}\boldsymbol{V}_L$ along with replacing $\boldsymbol{C}$ with $(1/2)\boldsymbol{C}$ for $k=\mathrm{NDZ}+1$ to yield

$$\boldsymbol{V}_{\mathrm{NDZ}+1}^{n+1}=\left[\frac{\Delta z}{\Delta t}\boldsymbol{R}_L\boldsymbol{C}+\boldsymbol{1}\right]^{-1}\left\{\left[\frac{\Delta z}{\Delta t}\boldsymbol{R}_L\boldsymbol{C}-\boldsymbol{1}\right]\boldsymbol{V}_{\mathrm{NDZ}+1}^{n} -2\boldsymbol{R}_L\left[\underbrace{\boldsymbol{I}_{\mathrm{NDZ}+1}^{n+1/2}}_{\boldsymbol{0}}-\boldsymbol{I}_{\mathrm{NDZ}}^{n+1/2}\right] -\frac{\Delta z}{\Delta t}\boldsymbol{R}_L\boldsymbol{C}\boldsymbol{A}_T\left[\mathcal{E}_0\left(t^{n+1}-\frac{\mathrm{NDZ}\Delta z}{v_z}\right)-\mathcal{E}_0\left(t^{n}-\frac{\mathrm{NDZ}\Delta z}{v_z}\right)\right] +\left[\boldsymbol{V}_L^{n+1}+\boldsymbol{V}_L^{n}\right]\right\}. \quad (65c)$$

Once the voltages are determined along the line for a particular time step, the currents are obtained from (63b) for $k=1,\cdots,$ NDZ as

$$\boldsymbol{I}_k^{n+3/2}=\boldsymbol{I}_k^{n+1/2}-\frac{\Delta t}{\Delta z}\left[\boldsymbol{V}_{k+1}^{n+1}-\boldsymbol{V}_k^{n+1}\right] +\boldsymbol{L}^{-1}\left[\frac{1}{v_z}\boldsymbol{A}_T-\boldsymbol{A}_L\right] \times\left[\mathcal{E}_0\left(t^{n+3/2}-\frac{(k-1/2)\Delta z}{v_z}\right)-\mathcal{E}_0\left(t^{n+1/2}-\frac{(k-1/2)\Delta z}{v_z}\right)\right]. \quad (65d)$$

For stability, the position and time discretizations must satisfy the Courant condition

$$\Delta t\le\frac{\Delta z}{v_{i\mathrm{MAX}}} \quad (66)$$

where $v_{i\mathrm{MAX}}$ is the maximum of the mode velocities. An equality in this expression is referred to as the "magic time step" [26].

VIII. Computed Results

The computed results compare the SPICE model, the time-domain to frequency-domain transformation and the finite-difference time-domain (FDTD) model. The structure is shown in Fig. 8 and consists of a 2-m length of ribbon cable. The wire radii are 7.5 mils, the dielectric thicknesses are 10 mils, and the dielectric constant is 3.5. In the case of inhomogeneous media as here, the incident fields should be computed with the conductors removed but with the dielectrics in place. However, for simplicity we will asume the incident field is with the conductors and insulations removed. The wires have center-to-center separations of 50 mils. The middle wire is chosen as the reference conductor, and a uniform plane wave is incident in the z direction with the electric field polarized in the x direction. The line is terminated in 500-Ω resistors giving

$$\boldsymbol{R}_S=\boldsymbol{R}_L=\begin{bmatrix}500 & 0\\ 0 & 500\end{bmatrix}.$$

The computed results will be for the near-end voltage of line 1, $V_1(0,t)$. The per-unit-length parameter matrices were computed with a numerical method and are

$$\boldsymbol{L}=\begin{bmatrix}0.7485 & 0.2408\\ 0.2408 & 0.7485\end{bmatrix}\ \mu\mathrm{H/m}$$
$$\boldsymbol{C}=\begin{bmatrix}24.982 & -6.266\\ -6.266 & 24.982\end{bmatrix}\ \mathrm{pF/m}.$$

This gives the mode velocities as

$$v_1=2.32398\times10^8\ \ \mathrm{m/s}$$
$$v_2=2.510645\times10^8\ \ \mathrm{m/s}.$$

The time form of the incident electric field $\mathcal{E}_0(t)$ is a ramp waveform rising to a level of 1 V/m with various rise times of $\tau_r=100$, 10, and 1 ns. This will illustrate cases where the rise time is greater than, on the order of, or less than the line one-way delays ($T_1=\mathcal{L}/v_1=8.606\,\mathrm{ns}, T_2=\mathcal{L}/v_2=7.966$ ns).

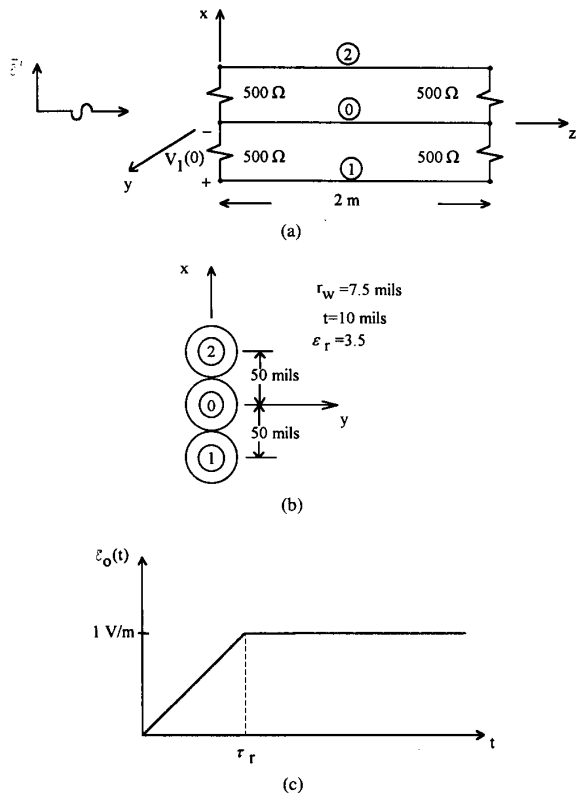

Fig. 8. Illustration of the problem configuration to be investigated by the methods. (a) The line and terminal configuration. (b) The cross-sectional dimensions. (c) The time waveform of the incident electric field.

The time-domain to frequency-domain transformation will be implemented by simulating the pulse as a periodic, 1-MHz trapezoidal waveform having a 50% duty cycle and equal rise and fall times that are equal to the rise time of the pulse. The spectrum of this waveform can be bounded as three segments: 0 dB/decade out to a frequency of $1/\pi\tau$ where τ is the pulsewidth, $-$ 20 dB/decade out to a frequency of $1/\pi\tau_r$ where τ_r is the pulse rise (fall) time, and $-$ 40 dB/decade thereafter [6]. The frequency response will be computed at harmonics of this waveform out to a point well above the second breakpoint of the spectrum. The time-domain response will be computed by combining the responses to these harmonics [25]. The finite-difference time-domain results will be computed by dividing the line into NDZ $= \mathcal{L}/\Delta z$ sections such that each section is no larger that 0.1λ at a point well above the second breakpoint of the spectrum using the smaller of the mode velocities to compute the wavelength. The time axis will be divided into NDT = Final Time$/\Delta t$ times such that the Courant condition in (66) is satisfied. This will be chosen at or slightly above the "magic time step" in order to show the stability and efficiency of the FDTD algorithm resulting in

$$\text{NDT} \geq \frac{(\text{NDZ})\,(\text{Final Time})\,(v_{i\max})}{\mathcal{L}}.$$

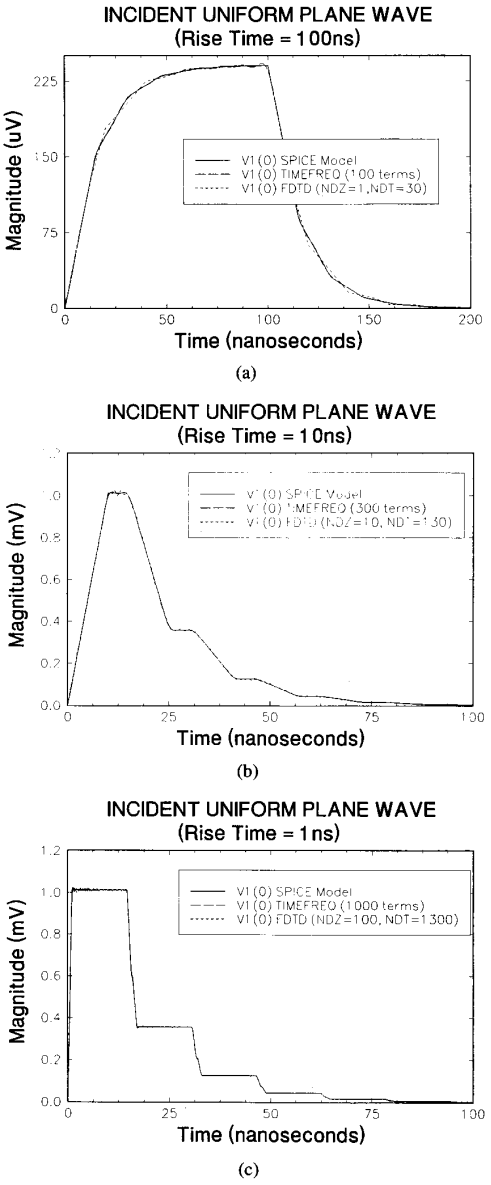

Fig. 9. Computed results comparing the results of the SPICE model, the time-domain to frequency-domain transformation method, and the finite-difference time-domain (FDTD) method. (a) Pulse rise time of 100 ns. (b) Pulse rise time of 10 ns. (c) Pulse rise time of 1 ns.

Fig. 9(a) shows the results for the 100-ns rise time. All three models show excellent correlation. Since the pulse rise time is substantially greater than the line one-way delays the resulting induced voltage waveform resembles the *derivative* of the incident field waveform and can be easily calculated using the simple model described in [6]. The time-domain to frequency-domain transformation utilized 100 harmonics of the 1-MHz trapezoidal pulse train. The spectrum of $\mathcal{E}_0(t)$ rolls off at $-$ 40 dB/decade above $1/\pi\tau_r = 3.18$ MHz [6]. Thus the time-domain to frequency-domain computation extends to approximately 30 times this second breakpoint of the spectrum.

The FDTD results were obtained by discretizing the line into NDZ $= \mathcal{L}/\Delta z = 1$ sections of length $\Delta z = \mathcal{L}/\text{NDZ} = 2$ m length, and the time into NDT $=$ Final Time$/\Delta t = 30$ time steps. Each section is $1/10\lambda$ at approximately 12 MHz which is a factor of 4 above the point where the waveform spectrum begins to roll off at $-$ 40 dB/decade. The magic time step occurs for NDT $= 25.11$ so the time axis division is approximately at the magic time step. This careful choice of discretization explains the reasonable accuracy of the FDTD algorithm and also demonstrates its efficiency.

The results for the 10-ns rise time are shown in Fig. 9(b). For the 10-ns rise time, all three models give excellent correlation. The spectrum of $\mathcal{E}_0(t)$ rolls off at $-$ 40 dB/decade above $1/\pi\tau_r = 31.8$ MHz so the time-domain to frequency-domain transformation method using 300 harmonics gives reasonably accurate results. The FDTD method uses NDZ $= 10$ and NDT $= 130$. Each section is $1/10\lambda$ at approximately 120 MHz which is again a factor of 4 above the point where the waveform spectrum begins to roll off at $-$ 40 dB/decade. The magic time step occurs for NDT ≥ 125.53 so the time axis division is on the order of the magic time step again demonstrating the convergence and efficiency of the algorithm. The results for the 1-ns rise time are shown in Fig. 9(c). The spectrum of $\mathcal{E}_0(t)$ rolls off at $-$ 40 dB/decade above $1/\pi\tau_r = 318$ MHz so the time-domain to frequency-domain transformation method using 1000 harmonics gives reasonably accurate results. The FDTD algorithm uses NDZ $= 100$ and NDT $= 1300$. Each section length is $1/10\lambda$ at approximately 1200 MHz. The magic time step occurs for NDT ≥ 1255.32. Again, this demonstrates the convergence and efficiency of the FDTD algorithm.

The SPICE model is not restricted to the time domain and can be used to give frequency-domain results although restricted to lossless lines. These are shown in Fig. 10 from 1 kHz to 200 MHz. The results of the frequency-domain direct calculation with and without losses are also shown. All three models give virtually identical results except around frequencies where the line is some multiple of a half wavelength.

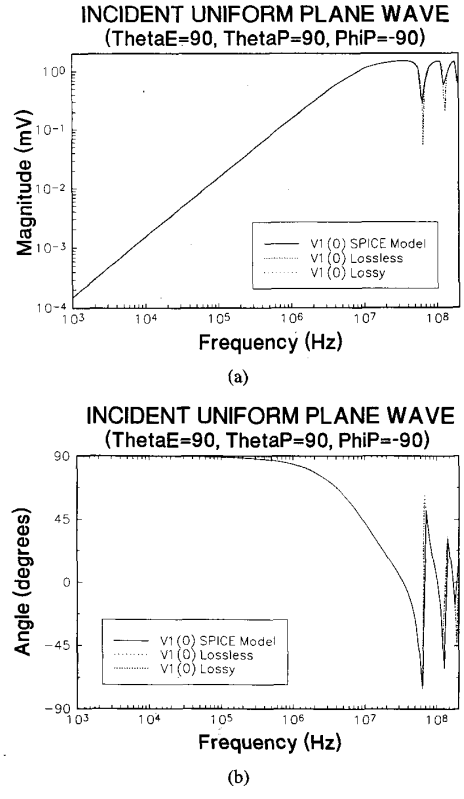

Fig. 10. Frequency-domain transfer functions. (a) Magnitude. (b) Phase.

IX. Summary and Conclusion

A simple model for predicting the time-domain response of a MTL to an incident electromagnetic field using the SPICE code or other similar circuit analysis codes was given. The model allows direct simulation of the time-domain response for various waveform shapes of the incident field and also allows the direct incorporation of nonlinear and dynamic terminations using the models already available in SPICE. The model can also be used to simulate cases where the field excitation is in the form of a lumped source at some point along the line as with a direct lightning stroke. This is done by simply dividing the line into sections to the left and right of the source location and modeling those lines with SPICE models without field illumination. The lumped incident field source can be simulated with the independent voltage and/or current sources available in SPICE at the common junction.

The comparison of the predictions of the SPICE model, the standard time-domain to frequency-domain transformation, and the FDTD algorithm gave similar results. However, the time-domain to frequency-domain method relied on superposition and is therefore restricted to linear loads although linear, dynamic loads may be included. The FDTD formulation presented here is restricted to linear, resistive loads. The SPICE model, although restricted to lossless lines can handle nonlinear as well as dynamic loads. The solution presented here is restricted to lossless lines in order to implement the model in SPICE. Lossy lines are evidently important in certain cases. However, diagonalization of the MTL equations for a lossy line in order to decouple them requires frequency-dependent modal transformations which is not easily implemented. So if a SPICE model is to be developed for the lossy line case, it appears that it will be considerably more complicated than the implementation proposed here.

References

[1] C. D. Taylor, R. S. Satterwhite, and C. W. Harrison, "The response of a terminated two-wire transmission line excited by a nonuniform electromagnetic field," *IEEE Trans. Antennas Propagat.*, vol. AP-13, pp. 987–989, Nov. 1965.

[2] A. A. Smith, Jr., "A more convenient form of the equations for the response of a transmission line excited by nonuniform fields," *IEEE Trans. Electromagn. Compat.*, vol. EMC-15, pp. 151–152, Aug. 1973.

[3] K. S. H. Lee, "Two parallel terminated conductors in external fields," *IEEE Trans. Electromagn. Compat.*, vol. EMC-20, no. 2, pp. 288–295, May 1978.

[4] S. Frankel, "Forcing functions for externally excited transmission lines," *IEEE Trans. Electromagn. Compat.* vol. EMC-22, no. 3, p. 210, Aug. 1980.

[5] A. A. Smith, *Coupling of External Electromagnetic Fields to Transmission Lines*, 2 nd ed. Interference Control Technologies, Inc., 1987.
[6] C. R. Paul, *Introduction to Electromagnetic Compatibility*. New York: Wiley Interscience, 1992.
[7] ——, "Application of multiconductor transmission line theory to the prediction of cable coupling–Vol. I—Multiconductor transmission line theory," Tech. Rep. RADC-TR-76-101 (A025028), Rome Air Development Center, Griffiss AFB, NY, Apr. 1976.
[8] ——, "Efficient numerical computation of the frequency response of cables illuminated by an electromagnetic field," *IEEE Trans. Microwave Theory Tech.*, vol. MTT-22, no. 4, pp. 454–457, Apr. 1974.
[9] ——, "Frequency response of multiconductor transmission lines illuminated by an incident electromagnetic field," *IEEE Trans. Electromagn. Compat.*, vol. EMC-18, no. 4, pp. 183–190, Nov. 1976.
[10] F. M. Tesche, T. K. Liu, S. K. Chang, and D. V. Giri, "Field excitation of multiconductor transmission lines," Tech. Rep. AFWL-TR-78-185, Air Force Weapons Lab., Albuquerque, NM, Feb. 1979.
[11] A. C. Cangellaris, "Distributed equivalent sources for the analysis of multiconductor transmission lines excited by an electromagnetic field," *IEEE Trans. Microwave Theory Tech.*, vol. 36, no. 10, pp. 1445–1448, Oct. 1988.
[12] G. W. Bechtold and D. J. Kozakoff, "Transmission line mode response of a multiconductor cable in a transient electromagnetic field," *IEEE Trans. Electromagn. Compat.*, vol. EMC-12, pp. 5–9, February 1970.
[13] A. K. Agrawal, H. J. Price, and S. H. Gurbaxani, "Transient response of multiconductor transmission lines excited by a nonuniform electromagnetic field," *IEEE Trans. Electromagn. Compat.*, vol. EMC-22, pp. 119–129, May 1980.
[14] C. W. Harrison, "Generalized theory of impedance loaded multiconductor transmission lines in an incident field," *IEEE Trans. Electromagn. Compat.*, vol. EMC-14, pp. 56–63, May 1972.
[15] C. R. Paul, "Applications of multiconductor transmission line theory to the prediction of cable coupling–Vol. VI—A digital computer program for determining terminal currents induced in a multiconductor transmission line by an incident electromagnetic field," Tech. Rep. RADC-TR-76-101 (A053560), Rome Air Development Center, Griffiss AFB, NY, Feb. 1978.
[16] C. R. Paul and R. T. Abraham, "Coupling of electromagnetic fields onto transmission lines: A comparison of the transmission line model and the method of moments," Tech. Rep. RADC-TR-82-286, vol. IV A, Rome Air Development Center, Griffiss AFB, NY, Nov. 1982.
[17] C. R. Paul and D. F. Herrick, "Coupling of electromagnetic fields to transmission lines," in *1982 IEEE Int. Symp. on Electromagnetic Compatibility*, (Santa Clara, CA, Sept. 1982).
[18] C. R. Paul and D. R. Bush, "Bounds on currents induced in transmission lines by incident fields," in *1984 IEEE SOUTHEASCON* (Louisville, KY, Apr. 1984).
[19] C. D. Taylor and J. P. Castillo, "On the response of a terminated twisted-wire cable excited by a plane-wave electromagnetic field," *IEEE Trans. Electromagn. Compat.*, vol. EMC-22, no. 1, pp. 16–19, Feb. 1980.
[20] E. F. Vance, *Coupling to Shielded Cables*. New York: Wiley, 1978.
[21] Y. Leviatan and A. T. Adams, "The response of a two-wire transmission line to incident field and voltage excitation, including the effects of higher order modes," *IEEE Trans. Antennas Propagat.*, vol. AP-30, no. 5, pp. 998–1003, Sept. 1982.
[22] G. E. Bridges and L. Shafai, "Plane wave coupling to multiple conductor transmission lines above a lossy earth," *IEEE Trans. Electromagn. Compat.*, vol. 31, no. 1, pp. 21–33, Feb. 1989.
[23] F. M. Tesche, "Plane wave coupling to cables," in *Handbook of Electromagnetic Compatibility*. San Diego, CA: Academic Press, 1994.
[24] C. R. Paul and S. A. Nasar, *Introduction to Electromagnetic Fields*, 2nd ed. New York: McGraw-Hill, 1987.
[25] C. R. Paul, "Literal solutions for time-domain crosstalk on lossless transmission lines," *IEEE Trans. Electromagn. Compat.*, vol. 34, no. 4, pp. 433–444, Nov. 1992.
[26] ——, "Incorporation of terminal constraints in the FDTD analysis of transmission lines," *IEEE Trans. Electromagn. Compat.*, vol. 36, no. 2, pp. 85–91, May 1994.
[27] D. E. Meriwether, "A numerical solution for the response of a strip transmission line over a ground plane excited by ionizing radiation," *IEEE Trans. Nucl. Sci.*, vol. NS-18, pp. 398–403, Aug. 1971.
[28] D. F. Higgins, "Calculating transmission line transients on personal computers," in *IEEE Int. Symp. on Electromagnetic Compatibility*, (Atlanta, GA, Aug. 25–27, 1987).
[29] E. S. M. Mok and G. I. Costache, "Skin-effect considerations on transient response of a transmission line excited by an electromagnetic pulse," *IEEE Trans. Electromagn. Compat.*, vol. 34, no. 3, pp. 320–329, Aug. 1992.

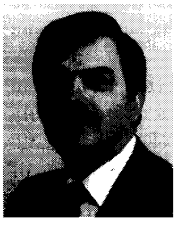

Clayton R. Paul (S'61–M'70–SM'79–F'87) was born in Macon, GA, on September 6, 1941. He received the B.S. degree fron The Citadel, Charleston, SC, in 1963, the M.S. degree from Georgia Institute of Technology, Atlanta, in 1964, and the Ph. D. degree from Purdue University, Lafayette, IN, in 1970, all in electrical engineering.

He has been a member of the faculty of the Department of Electrical Engineering at the University of Kentucky, Lexington, since 1971 and is currently Professor of Electrical Engineering. He is the author of seven textbooks on electrical engineering subjects and has published over 80 technical papers the majority of which are in his primary research area of Electromagnetic Compatibility (EMC) of electronic systems. From 1970 to 1984, he conducted extensive research for the US Air Force into modeling crosstalk in multiconductor transmission lines and printed circuit boards. From 1984 to 1990, he has served as a consultant to the IBM Corporation in the area of product EMC design.

Dr. Paul is a member of Tau Beta Pi and Eta Kappa Nu.